Time variant amplitude and phase dispersion correction for broadband data

Feng YANG (CGG), Ronan SABLON (CGG) and Robert SOUBARAS (CGG)*

Summary

Contrary to conventional seismic that focuses on a narrow band in middle frequencies, broadband seismic aims at acquiring information within the whole bandwidth emitted by the source. A good knowledge of the source signature is thus of paramount importance in broadband processing. However, the measurement of source signature is difficult and the modeling results are not satisfactory in the low frequencies. Another source of wavelet distortions is that seismic waves suffer from energy loss and phase dispersion due to intrinsic and apparent absorption which vary laterally and in depth. To address these challenges, a data-driven time variant non-Gaussian wavelet estimation which is sensible to phase is developed. As demonstrated on a North Sea broadband dataset, the proposed technique is able to produce zero-phase data on an enlarged bandwidth, both on low and high frequencies.

Introduction

In order to extract the full value of broadband seismic data in reservoir characterization, a simple and reliable way of broadband data zero-phasing is highly desirable (Dennis et al., 2000; White and Zabihi Naeini, 2014). Hampson and Galbraith (1981) had established a method to extract wavelet phase information on conventional seismic data by sonic log correlation. They observed that phase spectra were essentially linear over a limited bandwidth. Schakel and Mesdag (2014) have extended this method to broadband wavelet estimation. However, the assumption of linear behavior on phase spectrum over 6 octaves can be questionable.

In seismic processing, three main factors that determine the phase spectrum of the remaining wavelet are: (1) accuracy of far-field source signature; (2) velocity dispersion due to intrinsic absorption (White, 1975; Mavko, 1979) and apparent absorption related to multiple scattering in finely layered sediments (O'Doherty and Anstey, 1971); (3) the presence of remaining multiples.

Deriving an accurate far-field source signature is done early in the broadband processing flow since it has substantial impact on the processing steps that follow: source designature, receiver deghosting and demultiple. Various methods to obtain this source signature exist, each with their own advantages and drawbacks, such as modelling, direct measurement, reconstruction from near-field measurements or extraction from seismic data. The last two methods are currently the preferred solutions: cost-effective and producing overall accurate results. Combination of different tools has also been demonstrated to be a valuable road to derive accurate source signatures (Ni et al., 2014).

To compensate the absorption and dispersion effects in processing, currently, an inverse Q filtering under the assumption of constant Q material model (absorption coefficient is proportional to frequency, which implies absence or very weak absorption at low frequencies) is widely used in the industry (Wang, 2008). Xin and Hung (2009) have pushed this constant Q material model in three dimensions through a tomographic approach. As observed in laboratory measurements, Q is not constant in sandstone samples on seismic frequency range (Yao and Han, 2013): constant Q material model can be deficient for broadband seismic processing.

To our knowledge, a parametric Q model adequate for describing the absorption and dispersion phenomena over 6 octaves is not yet developed in the industry and the implementation (measurements to build this frequency dependent Q model from seismic data and application of this model on data) can be difficult. Therefore, a data-driven time variant deconvolution using non-Gaussian whitening technique is developed. Amplitude variation and phase dispersion are addressed simultaneously in our method.

Proposed method

The convolutional model is the basis to interpret the seismic traces in reflection seismology. Under this framework, the bandwidth of earth reflectivity that can be physically measured cannot exceed that of the source. Due to signal to noise consideration, the low frequency end is not deconvolved completely on pre-stack seismic data. The term "ultra-low frequency" used in this paper refers to this part of spectrum, generally situated from 1 Hz to 5 Hz on broadband data. On the high frequency end, the amplitude decay is predominantly governed by absorption.

Before deghosting, the amplitude spectrum of seismic is bell shaped. With the help of modern 3D deghosting algorithms (Soubaras, 2010; Poole, 2013; Wang, 2014), bell-shaped color filters due to receiver and source ghost effects are removed from seismic. The proposed whitening technique makes a step further: it aims to restore the true color of earth reflectivity by addressing the absorption and phase dispersion processes through blind deconvolution.

The conventional method to perform whitening is to apply a minimum phase operator on the seismic data to obtain the whitened reflectivity and estimate this operator by

DOI http://dx.doi.org/10.1190/segam2015-5859847.1

minimizing a cost function that is quadratic in the reflectivity. This method has the disadvantage that only time-invariant minimum phase distortions can be corrected. Another conventional whitening method is to apply a zero-phase operator, leaving the phase unchanged.

We want to be able to correct time-variant non-minimum phase distortions. In order to extract the phase and amplitude information from seismic data, the non-Gaussianity of earth reflectivity can be exploited (Sacchi 1997). Thanks to the removal of the ghosts, the seismic data is more closely linked to the reflectivity of the earth. The algorithms based on non-Gaussianity of earth reflectivity for phase estimation become thus significantly more stable and efficient on broadband data compared to conventional data. As both the phase and amplitude are estimated in the wavelet extraction process, the whitened seismic data is therefore naturally brought close to zero-phase.

The proposed method consists in applying a time-varying mixed-phase operator to the seismic data to obtain the whitened reflectivity and estimating this operator by minimizing a cost function which is non-quadratic in the reflectivity. A synthetic example is provided below to assess the power of our method.

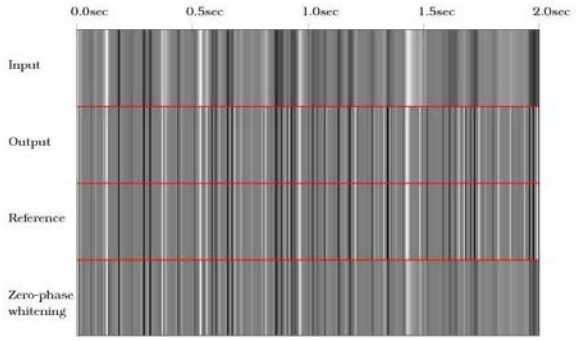

Figure 1: Input: reflectivity series with simulated phase dispersion due to the propagation in the earth; Output: recovered reflectivity using time variant non-Gaussian whitening; Reference: original reflectivity series; Zero-phase whitening: recovered reflectivity using zero-phase whitening (time invariant)

The original reflectivity series is plotted in Figure 1, labelled by "Reference". To simulate the phase dispersion due to wave propagation in the earth, phase dispersion on both the causal and anti-causal part of the wavelet has been added to produce the input seismic trace (shown on the top of Figure 1, labelled as "Input"). The deconvolved trace using time variant non-Gaussian whitening is plotted in Figure 1 labelled by "Output". As observed in Figure 1, the "Output" is virtually identical as the "Reference". For the sake of comparison, a zero-phase whitening result is shown at the bottom of Figure 1 (labelled by "Zero-phase whitening"). The initial correlation coefficient between the "Input" and the "Reference" is 0.64. This correlation coefficient increases to 0.81 for the "Zero-phase whitening" result and to 0.99 for the "Output" obtained by time variant non-Gaussian whitening.

Debubbling example on West Australia broadband data

The debubbling in broadband processing is a critical step to zero-phase the seismic data since bubble bounces create phase oscillations at the low frequencies. To address the bubble bounces precisely, the far-field source signature needs to be accurate.

By reducing the non-Gaussian whitening algorithm to its time invariant version, a data-driven residual debubbling can be performed to remediate the errors of source signature in bubble estimation. The assumption in this debubbling approach is that the amplitude spectrum of earth reflectivity is smooth. In practice, to meet this assumption, a sufficiently large temporal and spatial window is required.

The debubbling operator is thus derived through the following two steps as illustrated in Figure 2: (1) a whitening operator is estimated from seismic data using the non-Gaussianity of earth reflectivity (Sacchi 1997); (2) a re-coloring operator with a smooth amplitude spectrum approximating the original spectrum is calculated from this whitening operator using the method described by Soubaras (1990). Convolving the whitening operator and the re-coloring operator, one obtains the debubbling operator.

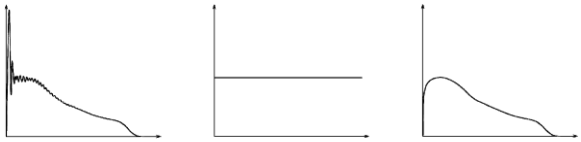

Figure 2: Schematic view of amplitude spectrum: (a) before debubbling; (b) after whitening; and (c) whitening followed by re-coloring. The horizontal axis corresponds to frequency while the vertical axis refers to amplitude.

An example is provided below to demonstrate the efficiency of our method. A modelled far-field signature has been used for debubbling. As commonly observed, the bubbles are badly estimated in a modelled signature. Consequently, residual bubbles are visible in Figure 3 (see zones indicated by arrows). The bubble effect is interestingly illustrated by a repetition (indicated by the arrow B) of an inclusion (encircled) in Figure 3. As the bubble energy concentrates on low frequencies, a low-pass filter (high cut at 20 Hz) is applied on seismic sections (see Figure 5 and 6) to better appreciate the bubble effects.

DOI http://dx.doi.org/10.1190/segam2015-5859847.1

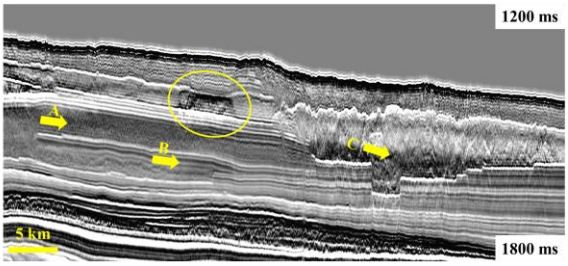

Figure 3: Broadband pre-stack time migrated seismic section of Australia's North-West shelf before residual debubbling.

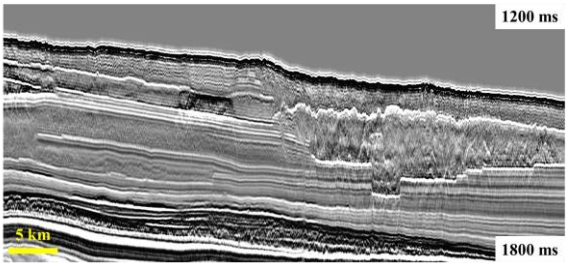

Figure 4: Debubbled section using a time invariant blind deconvolution.

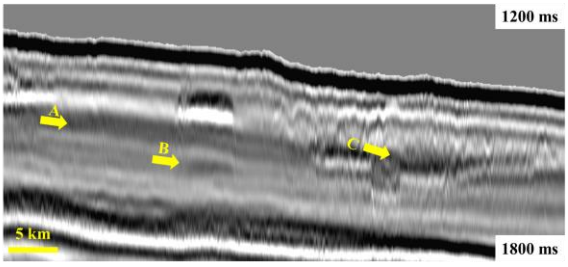

Figure 5: Seismic section of Figure 3 filtered by a low-pass filter.

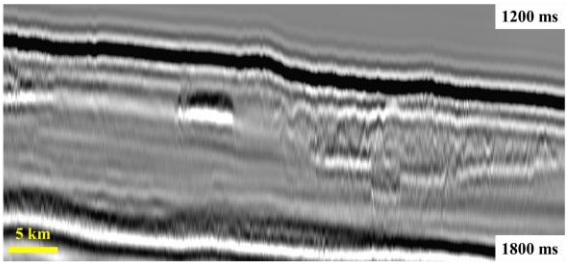

Figure 6: Seismic section of Figure 4 filtered by a low-pass filter.

Figure 6 shows clearly that the residual bubbles are nicely lifted off the data. Our algorithm can therefore be used for quality control of far-field source signature. The phase error due to residual bubbles is plotted in Figure 7. As observed from this curve, a rather large phase correction is necessary at low frequencies.

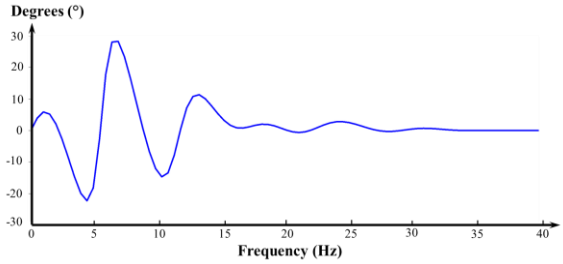

Figure 7: Phase spectrum of the residual debubbling operator.

Whitening example on North Sea broadband data

The seismic data was acquired in the region of the UK continental shelf Quadrant 20/05 using broadband variable-depth towed solid streamer (Soubaras 2010). This pilot 3D survey covered an area of 165 km^2. Processing was performed in early 2011 with the broadband processing tools and methods available at that time.

Time-variant non-Gaussian whitening technique has been applied post-stack on this 3D legacy cube. An inline section and a time-slice, before and after time-variant whitening are shown respectively in Figure 8 to 11. The seismic image after whitening becomes much sharper. This is a combination of three factors: (1) benefit of focusing effect due to zero-phasing (see the area pointed by yellow arrows in Figure 8 and 9); (2) enriched high frequencies which permit to resolve thin beds and subtle structures (see increased resolution for the separation of the Top Ekofisk and Tor doublet, encircled in Figure 8 and 9); (3) large-scale and subtle facies variations are captured by the recovered ultra-low frequencies (see time-slice comparison in Figure 10 and 11 at a two way time of 1128 ms below the sea surface). Amplitude spectra measured from the seismic sections before and after whitening are plotted in Figure 12. As already mentioned, both the two ends of the spectrum are whitened up to a certain extent determined by the signal to noise ratio. It is worth to note that the amplitude approaching zero frequency has been doubled. Compared to Figure 10, the time-slice shown in Figure 11 gets more contrasted thanks to the recovered ultra-low frequency content. Fine features and enhanced resolution are due to the enrichment in high frequencies.

The impedance contrast on longer distance (over 500 ms) has been successfully imaged using the recovered ultra-low frequency as shown in Figure 13 (enlarged view of the shallow part of the seismic section displayed in Figure 9) with well density log overlaid. The interpretation on stratigraphy sequence and major reflectors can be greatly eased with the response of ultra-low frequency. At large scale, darker blocks correspond to higher impedance while whiter blocks correspond to lower impedance.

DOI http://dx.doi.org/10.1190/segam2015-5859847.1

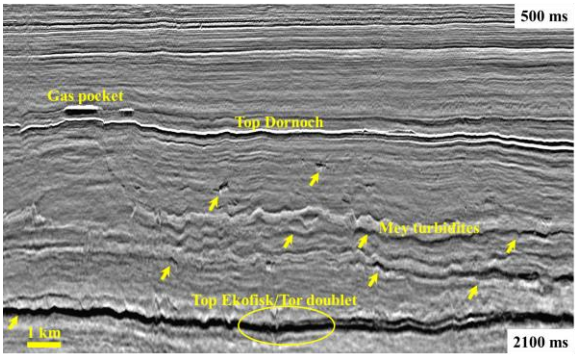

Figure 8: Inline section from the 3D legacy pre-stack time migrated cube (before time variant whitening).

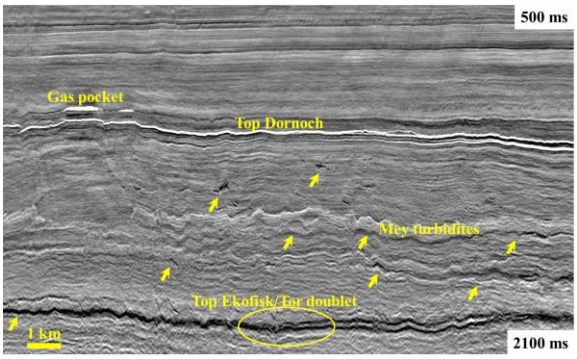

Figure 9: Inline section of Figure 8 after time variant whitening.

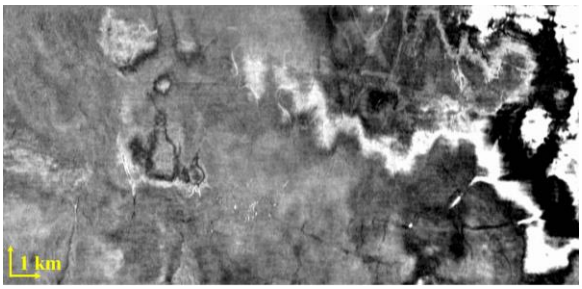

Figure 10: Time-slice at 1128 ms (two way time) before whitening.

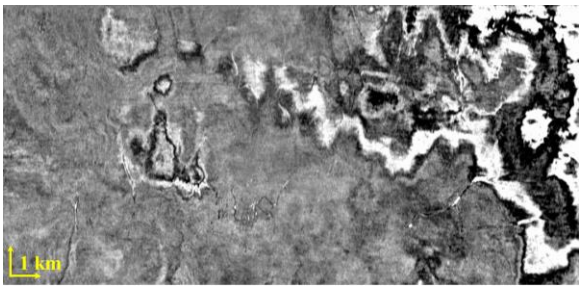

Figure 11: Time-slice at 1128 ms (two way time) after whitening.

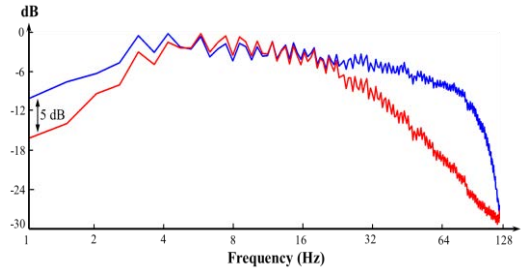

Figure 12: Normalized amplitude spectra in dB measured from the seismic sections shown in Figure 8 and 9 using a time window from 500 ms to 2100 ms. Amplitude spectrum before whitening is drawn in red while after whitening is plotted in blue.

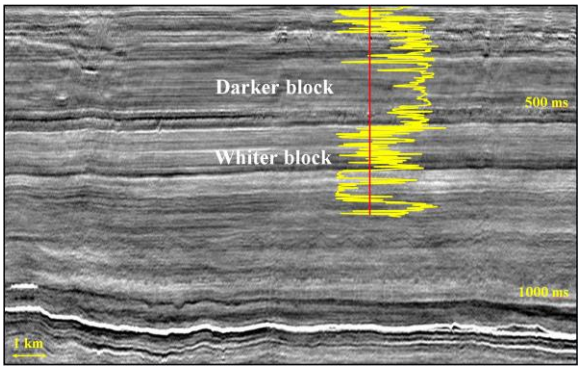

Figure 13: Enlarged view of the shallow part (two way time from 300 ms to 1200 ms) of the seismic section displayed in Figure 9 with well density log overlaid (well track is the vertical red line).

Conclusions

Broadband seismic data can be whitened at both the low frequency and high frequency ends of the spectrum, accompanied by a phase correction, using a time variant non-Gaussian whitening technique. On the high frequency end, the whitening result is similar to amplitude and phase compensation through inverse Q filtering. On the low frequency end, the amplitude recovery and phase correction achieved by the method proposed here is different. This method can be used for quality control of source far-field signature and phase monitoring of broadband data. Further comparisons with well logs are needed to assess the phase corrections brought by our method.

Acknowledgments

The authors thank Gregor Duval (CGG's multi-client data library) for providing the seismic data to conduct this project. Thierry Coleou (GeoConsulting, CGG), Jean-Philippe Coulon (GeoConsulting, CGG), and Menne Schakel (GeoSoftware, CGG) are greatly acknowledged for fruitful discussions.

DOI http://dx.doi.org/10.1190/segam2015-5859847.1

EDITED REFERENCES

Note: This reference list is a copyedited version of the reference list submitted by the author. Reference lists for the 2015 SEG Technical Program Expanded Abstracts have been copyedited so that references provided with the online metadata for each paper will achieve a high degree of linking to cited sources that appear on the Web.

REFERENCES

Dennis, L. P., F. M. Peterson, and T. I. Todorov, 2000, Inversion — The importance of low-frequency phase alignment: 70th Annual International Meeting, SEG, Expanded Abstracts, 1583–1586.

Duval, G., 2012, How broadband can unlock the remaining hydrocarbon potential of the North Sea: First Break, **30**, no. 12, 85–91.

Hampson, D., and M. Galbraith, 1981, Wavelet extraction by sonic-log correlation: Journal of the Canadian Society of Exploration Geophysicists, **17**, 24–42.

Mavko, G., E. Kjartansson, and K. Winkler, 1979, Seismic wave attenuation in rocks: Reviews of Geophysics, **17**, no. 6, 1155–1164. http://dx.doi.org/10.1029/RG017i006p01155.

Ni, Y., T. Payen, and A. Vesin, 2014, Joint inversion of near-field and far-field hydrophone data for source signature estimation: 84th Annual International Meeting, SEG, Expanded Abstracts, 57–61.

O'Doherty, R. F., and N. A. Anstey, 1971, Reflections on amplitudes: Geophysical Prospecting, **19**, no. 3, 430–458. http://dx.doi.org/10.1111/j.1365-2478.1971.tb00610.x.

Poole, G., 2013, Premigration receiver deghosting and redatuming for variable depth streamer data: 83rd Annual International Meeting, SEG, Expanded Abstracts, 4216–4220.

Sacchi, M. D., 1997, Reweighting strategies in seismic deconvolution: Geophysical Journal International, **129**, no. 3, 651–656. http://dx.doi.org/10.1111/j.1365-246X.1997.tb04500.x.

Schakel, M. D., and P. R. Mesdag, 2014, Fully data-driven quantitative reservoir characterization by broadband seismic: 84th Annual International Meeting, SEG, Expanded Abstracts, 2502–2506.

Soubaras, R., 1990, Deconvolution with pre-specified final wavelet length: 60th Annual International Meeting, SEG, Expanded Abstracts, 1665–1669.

Soubaras, R., 2010, Deghosting by joint deconvolution of a migration and a mirror migration: 80th Annual International Meeting, SEG, Expanded Abstracts, 3406–3410.

Wang, Y., 2008, Seismic inverse Q-filtering: Wiley-Blackwell.

Wang, P., S. Ray, and K. Nimsaila, 2014, 3D joint deghosting and crossline interpolation for marine single-component streamer data: 84th Annual International Meeting, SEG, Expanded Abstracts, 3594–3598.

White, J. E., 1975, Computed seismic speeds and attenuation in rocks with partial gas saturation: Geophysics, **40**, 224–232. http://dx.doi.org/10.1190/1.1440520.

White, R., and E. Zabihi Naeini, 2014, Broadband well-tie: 76th Annual International Conference and Exhibition, EAGE, Extended Abstracts, http://dx.doi.org/10.3997/2214-4609.20140749.

Xin, K., and B. Hung, 2009, 3D tomographic Q-inversion for compensating frequency-dependent attenuation and dispersion: 79th Annual International Meeting, SEG, Expanded Abstracts, 4014–4018.

DOI http://dx.doi.org/10.1190/segam2015-5859847.1

Yao, Q., and D.-H. Han, 2013, Progresses on velocity dispersion and wave attenuation measurements at seismic frequency: 83rd Annual International Meeting, SEG, Expanded Abstracts, 2883–2888.

DOI http://dx.doi.org/10.1190/segam2015-5859847.1